Early Hydration and Viscoelastic Properties of Tricalcium Aluminate Pastes Influenced by Soluble Sodium Salts

Daniel Axthammer[1,2], Tobias Lange[1], Joachim Dengler[2] and Torben Gädt[1,*]

[1] Chair for Chemistry of Construction Materials, TUM School of Natural Sciences, Department of Chemistry, Technical University of Munich, Lichtenbergstraße 4, 85748 Garching, Germany

[2] BASF Construction Additives GmbH, Dr.-Albert-Frank-Straße 32, 83308 Trostberg, Germany

[*] Contact: torben.gaedt@tum.de

Abstract

During the early hydration of ordinary Portland cement (OPC), tricalcium aluminate (C_3A) exhibits the highest reactivity among the clinker phases. Consequently, C_3A significantly influences the early rheological properties of OPC-based materials, thereby linking rheology with C_3A reactivity. The reactivity of C_3A is affected by temperature, calcium sulfates, admixtures, and ionic strength. Calcium sulfate phases such as gypsum, bassanite, or anhydrite are used in technical Portland cement to control the early reactivity of C_3A.

This work investigates the impact of three sodium salts - sodium chloride (NaCl), sodium nitrate ($NaNO_3$), and sodium sulfate (Na_2SO_4) - on the hydration of C_3A. We study model suspensions composed of 10% cubic C_3A and 90% quartz by weight with in-situ isothermal calorimetry. The C_3A suspensions were mixed inside the calorimeter with a water-to-solid ratio of 0.8. Increasing concentrations, i.e., 400, 1000, and 2000 µmol g^{-1}, of the sodium salts mentioned above lead to characteristically decreased C_3A reactivities. Combined with small amplitude oscillatory shear (SAOS) rheology experiments, we show that the addition of Na_2SO_4 significantly reduces the heat flow and the initial storage modulus. In contrast, $NaNO_3$ and NaCl had less pronounced effects on both storage modulus and reaction heat.

The differences in structure development are attributed to the formation of different hydrate phases. Specifically, Na_2SO_4 leads to ettringite formation, whereas the presence of nitrate and chloride ions

favors the precipitation of AFm phases. The study concludes that introducing various sodium salts can modulate the kinetics of C_3A hydration and alter the reaction pathway, forming different hydrate phases.

1 Introduction

The reactivity of the cementitious binder in the first minutes of hydration is crucially important for the fresh properties of concrete. Therefore, a more comprehensive understanding of the initial reactions of the main ordinary Portland cement (OPC) components is relevant for precisely controlling the hydration kinetics and the rheological parameters of (blended) cements.

The early viscoelastic properties of OPC-based materials, such as concrete, are significantly influenced by the reactions involving tricalcium aluminate (C_3A) [1–3]. In the first minutes of hydration, the reaction of C_3A, which typically constitutes up to 10 wt.% of OPC [4, 5], with water leads to the precipitation of calcium-aluminate-hydrates (C-A-H, AFm phases). If not adequately controlled, this process results in a swift decline in workability. This phenomenon, known as a flash set, is attributed to the formation of AFm phases (C_2AH_8 and C_4AH_{13}), which form as platelets, causing rapid stiffening of the paste [4, 6]. Over time, the metastable AFm phases undergo partial or complete transformation into the more stable hydrate phase katoite (or hydrogarnet, C_3AH_6) [7–11].

Calcium sulfate sources like gypsum or anhydrite are added during clinker grinding to act as set-retarding agents [12, 13]. This addition not only slows down the initial C_3A reaction, thereby preventing a flash set but also redirects the hydration pathway of C_3A towards ettringite formation [10, 14]. The retardation of the early C_3A hydration in the presence of calcium sulfate is attributed largely due to the adsorption of sulfate or calcium sulfate ion-pair complexes [6, 15–19]. The precipitation of ettringite significantly impacts the initial material characteristics, particularly the rheological properties of OPC-based pastes and mortars. Jakob et al. demonstrated the critical role of ettringite in the early-stage rheology of OPC pastes [1], and Gołaszewski showed that the yield value of mortars is influenced by the conversion of C_3A to ettringite [2]. Furthermore, the static yield stress of a model cement pastes containing C_3A and C_3S depends exponentially on the C_3A phase content of the model cement [20].

In addition to the sulfate ions of the sulfate carriers, other inorganic ions, such as nitrate, can be present in the pore solution. Accelerators or corrosion inhibitors are typical sources of nitrate ions. Ions such as chloride or nitrate can be incorporated into the layered double hydroxide (LDH) structure of AFm phases, resulting in the formation of Friedel's salt and nitrate AFm [21–24]. In a recent study, Li and colleagues employed a combination of inorganic and organic molecules to selectively control the hydration process of aluminate phases in OPC. Their approach involved the retardation of ettringite nucleation and the simultaneous enhancement of aluminates dissolution at a specific point in time, resulting in a higher amount of ettringite formed and improved material properties [25]. Thus, understanding how ions like SO_4^{2}, Cl^- or NO_3^- affect the hydration kinetics of C_3A is important for elucidating their influence on

the early age rheology and structure of cementitious materials.

The kinetics, morphology, and spatial distribution of hydrate formation exert a significant influence on the viscoelastic properties of fresh cementitious systems [1, 26–28]. Small amplitude oscillatory shear (SAOS) tests have emerged as a suitable, non-destructive technique to study the viscoelastic behavior of fresh cementitious pastes [29].

In SAOS testing, a material is exposed to a very small sinusoidal strain, and its stress response, represented by the complex modulus ($G^* = G' + iG''$), is measured. The storage modulus (G') characterizes the material's elastic response, while the loss modulus (G'') reflects its viscous behavior. Within the linear viscoelastic regime (LVR), the storage modulus remains constant, unaffected by the strain amplitude [30]. For cementitious systems, the time-dependent evolution of G' provides insights into colloidal interactions (short-term, seconds) or structure build-up due to precipitating hydrate phases [29].

Various studies have employed SAOS measurements to explore the structural evolution of cementitious pastes over time [26, 31–34]. Huang et al., for instance, investigated the impact of gypsum content in C_3A-gypsum pastes on their structural development, finding that increased ettringite formation leads to a higher storage modulus after 300 min of hydration [27]. Roussel et al. demonstrated how C-S-H precipitation in fresh cement pastes contributes to rigidification, significantly influencing the evolution of G' [28]. Additionally, Han et al. conducted SAOS tests to analyze C_3A hydration's role in the structural development of cement paste. They identified two primary factors for early structural build-up: colloidal interactions among flocculated particles and cohesion between ettringite particles [35]. These findings underscore SAOS testing as a valuable method for investigating the viscoelastic properties of cementitious pastes, particularly for non-destructively studying the structural development induced by hydrate phase precipitation.

This study investigates the early-stage hydration kinetics and viscoelastic properties of tricalcium aluminate (C_3A) suspensions in various sodium salts. Specifically, we seek to:

1. Examine the effects of sodium chloride (NaCl), sodium nitrate ($NaNO_3$), and sodium sulfate (Na_2SO_4) on the hydration behavior of C_3A and its subsequent impact on the structural development of cementitious pastes.

2. Utilize in-situ isothermal calorimetry, small amplitude oscillatory shear (SAOS) tests, and XRD to monitor the heat flow, the viscoelastic properties of C_3A suspensions and the phase development for the different sodium salts at three different concentrations.

3. Investigate the connection between the hydrate phase formation and the rheological properties of the pastes.

In summary, we intend to provide deeper insights into the modulation of C_3A hydration kinetics and the early structural properties. Such understanding is helpful for a pure OPC-based system and composite binders containing supplementary cementitious materials.

2 Materials and Methods

2.1 Materials

The chemicals were commercially sourced and were used without further purification: $CaCO_3$ (99.3 %), Al_2O_3 (99.7 %), calcium aluminate cement (27 % CaO and 72 % Al_2O_3), SiO_2 powder (98.0 %), Na_2SO_4 (99.0 %), NaCl (99.5 %) and $NaNO_3$ (99.5 %).

2.1.1 Synthesis of cubic C_3A

Cubic C_3A was synthesized according to a recently developed protocol [36]. Briefly, C_3A was prepared by sintering cylindrical green bodies composed of $CaCO_3$, Al_2O_3, calcium aluminate cement and water (water-to-solid ratio w/s = 0.5) in stoichiometric amounts (Ca/Al ratio = 1.5) twice at 1400 °C. The detailed synthesis procedure and characterization can be found elsewhere [36]. The purity of 99.6 wt.% of the prepared cubic C_3A sample (mayenite: 0.3 wt.%, lime: 0.1 wt.%) was confirmed by XRD accompanied by Rietveld refinement (R_{wp} = 5.64 %, GOF = 1.74).

2.1.2 C_3A model system (C_3A MS)

Due to the comparatively high reactivity of C_3A, researchers typically conduct studies with diluted systems (Minard et al., Pourchet et al.: w/s = 25; Myers et al.: w/s = 10) [7, 17, 37] or regulate the reactivity by adding calcium sulfate when examining pure cubic C_3A [9, 38]. Our study aims to investigate the impacts of sodium salts in the absence of calcium sulfate and other clinker phases. To achieve this, we use a C_3A model system consisting of a combination of cubic C_3A and quartz filler. This enables the examination of the hydration behavior of C_3A and the impact of hydrate precipitation in a system having a particle size distribution similar to OPC without disturbance from other reactions, such as the hydration of silicate phases (C_3S or C_2S).

A C_3A model system (10 wt.% cubic C_3A / 90 wt.% quartz powder) was used for isothermal heat flow calorimetry, small amplitude oscillatory shear testing, and in-situ XRD measurements. The model

system's particle size distribution (PSD) was chosen to be in the range of commercial ordinary Portland cements. The particle sizes were determined by laser diffraction analysis using a CILAS 1064 Particle Size Analyzer, and the resulting PSD is shown in Figure 1. The characteristic values were determined to $d_{50} = 12.26\,\mu m$, $d_{90} = 40.38\,\mu m$ for the synthesized C_3A and $d_{50} = 11.08\,\mu m$, $d_{90} = 35.14\,\mu m$ for the C_3A MS.

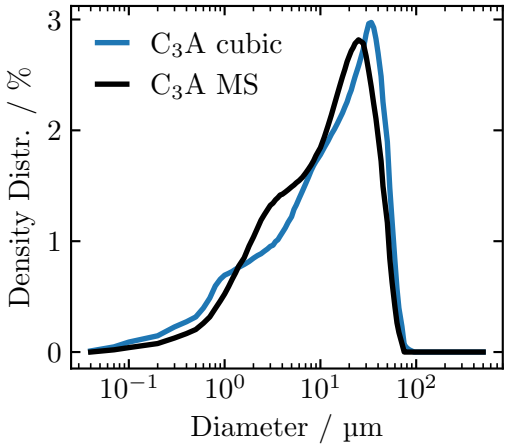

Figure 1: Particle size distribution of the synthesized cubic C_3A and the prepared C_3A model system with quartz powder.

The C_3A model system was prepared by weighing 50 g cubic C_3A and 450 g SiO_2 powder in a plastic bottle. Subsequently, this mix was tumbled in an overhead shaker (Heidolph REAX 20) at 15 rpm for 2 h. Afterward, the powder was co-milled in a rotary ball mill (AAM-WA 350, AAM Mahltechnik, Germany) equipped with 3 kg ZrO_2 grinding balls (diameter = 21 mm) at 50 rpm for 20 min for further homogenization. The sample was filled into a tightly sealed plastic bottle and was stored in a desiccator under a vacuum over silica gel until further use.

2.1.3 Model systems with sodium salts

All following experiments were performed using the C_3A MS and at a water-to-solid ratio (w/s) 0.8. This relatively high amount of water was necessary to obtain a pasty texture of the mixtures. The smooth consistency guarantees good workability during sample mixing and spreading and allows optimal trimming during preparation for the SAOS experiments and in-situ XRD measurements. The aqueous sodium salt solutions were prepared before each measurement and according to dosages of 400, 1000, and 2000 $\mu mol\,g^{-1}$ C_3A by mixing the sodium salts with Milli-Q water. The dosages of 400, 1000 and 2000 $\mu mol\,g^{-1}$ C_3A of the salts are equivalent to 10.8, 27.0 and 54.0 mol % (mol of the salts per mol C_3A). For comparison, the complete conversion of 1 equivalent of C_3A to ettringite requires 3 equivalents of $CaSO_4$, or 300 mol % (11 111 $\mu mol\,g^{-1}$) of calcium sulfate. In OPC, with typical amounts

of approximately 5 wt.% C_3A and 3 wt.% SO_3, a ratio of 200 mol % (7410 µmol g^{-1}) is found. Therefore, the amount of salts used in this study is less than that of calcium sulfate typically used to control the reactivity of C_3A in OPC.

2.2 Small amplitude oscillatory shear test (SAOS)

To investigate the structural build-up of the C_3A pastes in the presence of the sodium salts, oscillatory time sweeps were performed on a rotational rheometer (MCR 302e, Anton Paar, Austria) at 20 °C. The pastes were tested with a plate-plate geometry (PP25/P2, diameter = 25 mm). Both plates were serrated to prevent wall slippage during the measurements [39]. All measurements were conducted with a gap size of 1.00 mm at a constant shear strain ($\gamma = 10^{-4}$) and at a constant angular frequency ($\omega = 1\,\mathrm{rad\,s^{-1}}$) for 3 h. The chosen strain is within the LVR of the C_3A model suspensions. The groove on the bottom plate was filled with deionized water, and the measuring geometry was covered with a hood to avoid evaporation during the experiments. The storage modulus (G') represents the elastic portion of the shear modulus and is proportional to the energy stored when the material is subjected to oscillatory shear. On the other hand, the viscous contribution is described by the loss modulus (G''), and this factor is determined by the energy dissipated during the measurements [30, 33]. In all experiments, G'' was found to be more than one order of magnitude smaller than G' over the entire duration of the measurements, resulting in a loss factor that was below 1 (Supporting Information Figures S3, S4). The evolution of the storage modulus was used as an indicator of the structural build-up of the pastes due to hydrate precipitation during the hydration process.

For the SAOS measurements, 10.0 g of the C_3A MS was weighed into a plastic cup, and DI water or the salt solutions were added according to the dosages described before. The mixture was stirred for 1 min at 600 rpm by a mechanical stirrer equipped with a propeller paddle. An appropriate amount of the pastes was immediately placed on the serrated bottom plate. The measurements started at 2 min 30 s after the addition of solutions and were carried out continuously for 3 h.

2.3 Isothermal calorimetry

The reaction heat during the hydration of C_3A/quartz model systems in the presence of the sodium salts was measured on an eight-channel isothermal calorimeter (TAM Air, TA Instruments, USA) at 20 °C. Custom mixers (Bohr-O-Mir 4000, Technisch Zeichnen Grassl, Germany)[40] equipped with three T-shape paddles in a planetary mixer configuration were used. allowing the addition of solutions and mixing of pastes in the calorimeter. The sample vials were composed of a plastic/graphite composite,

and the mixers were driven by an electrical motor at 600 rpm. For each experiment, 3.0000(5) g of the C_3A MS was weighed into the sample vials. The solutions were prepared according to the desired dosages and were weighed into the three syringes corresponding to a w/s of 0.8 and a precision of ±0.5 mg. The syringes and sample vials were mounted on the in-situ mixers and placed in the calorimeter for thermal equilibration at the calorimeter temperature of 20 °C overnight. Quartz sand with the same heat capacity as the samples was used as a reference sample. After baseline determination, the powder was pre-mixed for 10 s, the solution was injected, and stirring was continued for 60 s. Experiments were run for 3 h, and the heat flow data was normalized to the C_3A content of the suspensions.

2.4 Thermodynamic modeling

We used Reaktoro [41] in combination with the Cemdata18 database [42] to calculate the thermodynamic equilibria for the combinations of the sodium salts and the C_3A model system. The equilibrium composition of the different mixes was calculated for different C_3A hydration degrees. Since the experiments were conducted at room temperature, microcrystalline $Al(OH)_3$ was allowed to precipitate during the modeling [42, 43]. Since the formation of katoite (C_3AH_6) is kinetically hindered at room temperature, it was not allowed to precipitate during the modeling, as the experiments (SAOS and calorimetry) were only run for 3 h [8, 10]. $C_2AH_{7.5}$ was used as thermodynamic product instead of C_2AH_8, as C_2AH_8 is not included in the Cemdata18 database [42]. During the reaction of Na_2SO_4 and C_3A, the U-phase ($4\,CaO \cdot 0.9\,Al_2O_3 \cdot 1.1\,SO_3 \cdot 0.5\,NaO \cdot 16\,H_2O$), a sodium-substituted AFm phase could also theoretically precipitate [38, 44, 45]. However, this phase was not identified during in-situ XRD experiments, so it was excluded from subsequent thermodynamic modeling.

2.5 In-situ X-Ray Diffraction

The precipitation of the hydrate phases during hydration was followed by in-situ XRD. Diffractograms were recorded by using a Bruker D8 Advance diffractometer equipped with a Cu-source and a VÅNTEC-1 detector (12° 2θ detector opening). The diffractometer optics consisted of a divergence slit with 0.2° and primary and secondary soller slits of 2.5°.

Pastes were prepared the same way as for the SAOS measurements and filled in the sample holder immediately after mixing. The pastes were covered with a 7.5 µm thick polyimide film to prevent water evaporation during the measurements. Starting at 10 min after mixing, a diffractogram was collected every 15 min ($7-50°$ 2θ). The in-situ XRD measurements were carried out for a total duration of 3 h.

The following structure files with ICSD codes were utilized for analyzing the relevant phases through

qualitative methods with the Topas-Academic V7 software [46]. C_3A cubic (1841) [47], quartz (174) [48], ettringite (155395) [49], Friedel's salt ($C_4ACl_2H_{10}$, 62363) [50], nitrate AFm ($C_4A(NO_3)_2H_{10}$, 280171) [51], monocarbonate (MCB, 59327) [52], and hemicarbonate (HCB, 263124) [53]. Additionally, a hkl-Phase model adapted from Goergens et al. for C_2AH_x was used to describe the precipitating C_2AH_8 phase [54]. hkl-Phase models, according to Bergold et al., were used to model the residual water and the Kapton film during in-situ XRD [55].

2.6 Hydration stoppage and scanning electron imaging

The pastes used for scanning electron microscopy (SEM) experiments were prepared following the same procedure as for SAOS and in-situ XRD measurements. The pastes were stored in tightly sealed plastic cups with a wet cloth between the lid and the cup to prevent evaporation during the hydration process. Hydration was stopped using the solvent exchange method with isopropanol, following the recommendations of Mantellato et al. and Snellings et al. [56, 57]. After 3 h, 5 g of the pastes were immersed in 50 mL of cold isopropanol. The mixture was stirred for 15 min. The mixture was then poured onto a Büchner filter equipped with a polyamide filter (mesh size 0.20 µm), and the isopropanol was removed. The residue was rinsed twice using cold isopropanol. The filter paper and residue were placed in a crystallization dish and dried for two days at room temperature under a dry nitrogen flow. Electron micrographs were captured using a Hitachi TM1000 scanning electron microscope at 15 kV acceleration voltage and a magnification of 5000. Before imaging, the samples were coated with a gold layer to improve the samples' conductivity and avoid charge artifacts.

3 Results and Discussion

3.1 Early Reactivity of C_3A with Sodium Salts – Heat of Hydration

The intricate dynamics of C_3A paste hydration are not trivial to study, especially in the first few minutes. In-situ isothermal calorimetry provides experimental insight into the very early hydration kinetics. We mixed pastes containing C_3A and quartz (10 wt.%/90 wt.%) in the calorimeter by adding an aqueous solution containing either Na_2SO_4, NaCl or $NaNO_3$. The observed cumulative heats over 3 h of hydration in the absence and presence of the three sodium salts at dosages of 2000 µmol g^{-1} are displayed in Figure 2 on the left. The complete set of raw data of the calorimetric experiments is provided in the Supporting Information (Figure S1). The addition of the sodium salts decreases the early heat compared to the reference sample of C_3A that was hydrated solely in pure water. Although

other authors [16, 58] have reported sodium sulfate as the least effective of various alkali sulfates in reducing the dissolution rate of C_3A, our findings show a significant decrease in early heat in the presence of Na_2SO_4. The heat of hydration after 3 h is reduced from 893.6 J g^{-1} (reference) to 596.1 J g^{-1} with $NaNO_3$, 578.9 J g^{-1} with NaCl and 323.2 J g^{-1} with Na_2SO_4. $NaNO_3$ and NaCl modified the hydration kinetics to a comparable extent. The presence of Na_2SO_4 has the most significant effect on the hydration rate of the C_3A suspension.

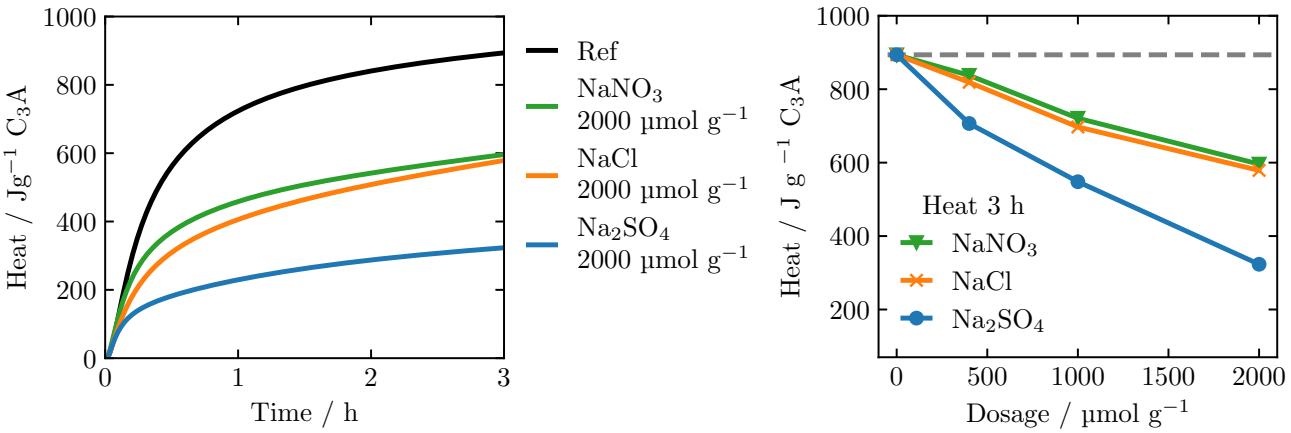

Figure 2: Left: Cumulative heat over 3 h of hydration of the C_3A MS in pure water (Ref) and in the presence of the three sodium salts at dosages of 2000 µmol g^{-1} C_3A. Right: Cumulative heat for different salt dosages after 3 h of hydration. In the absence of sodium salts, the cumulative heat determined after 3 h is marked as a dashed gray line.

To assess the impact of increasing sodium salt dosages on C_3A hydration, we plotted the cumulative heat at 3 h against the respective dosages (Figure 2 right). Increasing the salt dosage from 400 to 1000 and 2000 µmol g^{-1} caused an approximately linear decrease in heat after three hours for all three tested salts. The heat decreases in the presence of NaCl and $NaNO_3$ are similar but significantly smaller than for Na_2SO_4. The highest dosage of 2000 µmol g^{-1} of Na_2SO_4 reduced the heat after 3 h by almost 65 %. To summarize, the sodium salts reducing the heat after 3 h in the following order: $NaNO_3 \approx NaCl < Na_2SO_4$.

3.2 Structural Build-Up – Small Amplitude Oscillatory Shear (SAOS) Tests

We determined the structural evolution of C_3A pastes (comprising 10 wt.% C_3A, 90 wt.% quartz, and a water-to-solid ratio of 0.8) during hydration using oscillatory SAOS tests. These tests were performed at a strain of 10^{-4} and an angular frequency of 1 rad s^{-1}, in both the absence and presence of sodium salts. The selected strain was within the linear viscoelastic regime (LVR) of the C_3A pastes. Figure 3 illustrates two examples, showing the evolution of storage and loss moduli for C_3A hydrating in pure water (Ref, black) and with sodium sulfate (2000 µmol g^{-1}, blue). In both systems, representing our study's highest

and lowest initial storage moduli, the storage modulus measurements consistently exceeded the loss modulus throughout the experiments. The loss factor, i.e., the G''/G' ratio, remained below 1 for all samples (Supporting Information Figure S4), suggesting that the samples' elastic behavior was dominant. Hence, the evolution of the storage moduli serves as a reliable indicator of structural build-up in the C_3A pastes.

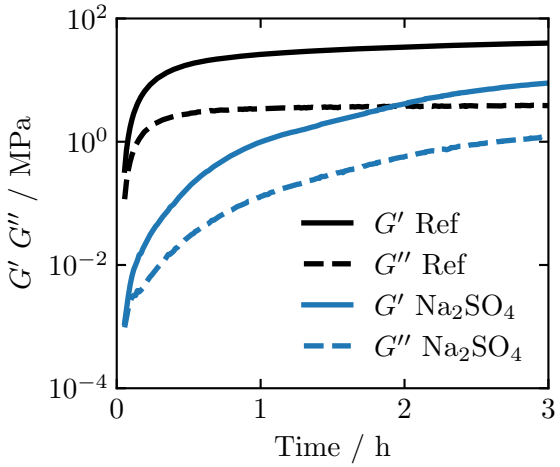

Figure 3: Development of storage modulus G' (solid lines) and loss modulus G'' (dashed lines) for C_3A MS hydrating in pure water (Ref, black) and in the presence of sodium sulfate (2000 µmol g^{-1} C_3A, blue).

Figure 4 displays the storage modulus development over 3 h for C_3A MS in pure water (Ref) and with various sodium salts ($NaNO_3$, NaCl, and Na_2SO_4) at 2000 µmol g^{-1}. The addition of Na_2SO_4 reduces the initial storage modulus from 0.35 MPa to 1.15×10^{-3} MPa, a reduction of more than two orders of magnitude compared to the reference. Sodium chloride and nitrate moderately reduce the storage modulus during the initial minutes of hydration. The order of the sodium salts' impact on the early storage modulus of the C_3A paste is as follows: nitrate < chloride < sulfate. During the first 3 h, G' increases by nearly four orders of magnitude in the presence of sodium sulfate, a more significant change than observed in the reference and C_3A paste with sodium nitrate and chloride.

To further clarify the effect of varying sodium salt dosages, we plotted the storage modulus G' at the age of 3 min and after 3 h against each salt's dosage (Figure 5). A significant decrease in the initial storage modulus was observed with increasing dosages of sodium sulfate. The addition of NaCl at 400 µmol g^{-1} led to an 84 % initial reduction in G', followed by only modest additional reductions at higher dosages. Finally, the initial storage moduli for all $NaNO_3$ containing samples were also lower than the reference. At the lower concentrations of 400 µmol g^{-1} and 1000 µmol g^{-1}, the reduction is small but reaches 74 % at the highest dosage of 2000 µmol g^{-1}.

After three hours of hydration, the reference mixture reached a storage modulus of 40 MPa. The

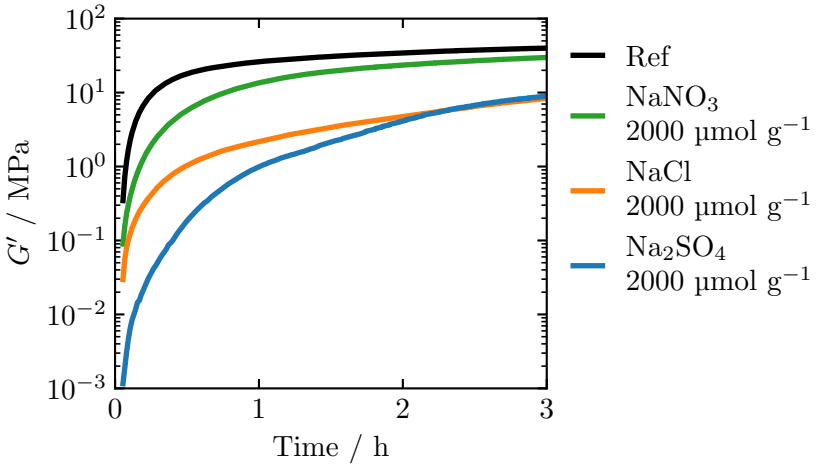

Figure 4: Development of the storage modulus (G') over 3 h of hydration of C_3A MS in pure water (Ref) and in the presence of sodium salts ($NaNO_3$, NaCl, and Na_2SO_4) at 2000 µmol g^{-1} C_3A.

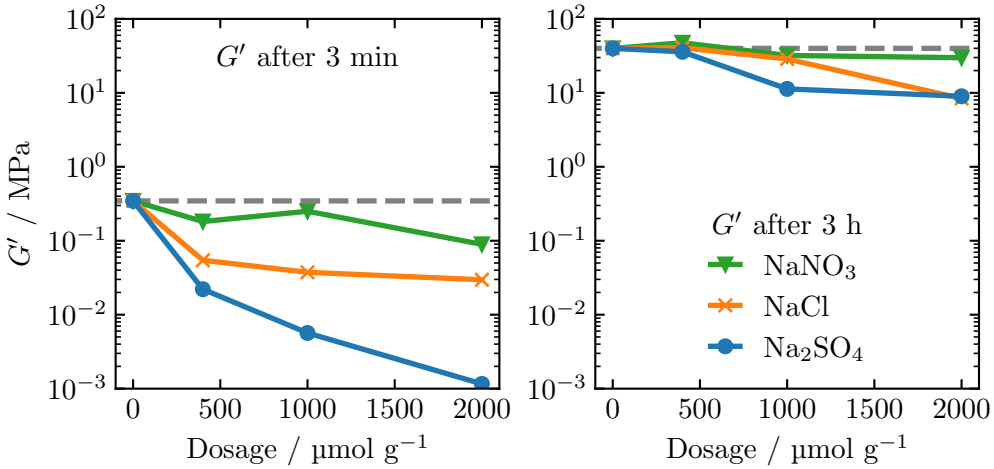

Figure 5: Storage Modulus after 3 min (left) and 3 h (right) of hydration of C_3A MS, dependent on the dosage of $NaNO_3$, NaCl, and Na_2SO_4. The storage moduli determined in the absence of sodium salts are marked as dashed gray lines. The y-axis was scaled to equal values for both times to compare the increase in G' over the SAOS measurement duration.

relative differences between the samples are significantly smaller than those for the initial G' values at 3 min. The highest dosage of Na_2SO_4 resulted in the smallest G' value of approx. 9 MPa. The 3 h storage modulus was only minimally affected by higher salt dosages. These findings confirm that the very early viscoelastic properties of the C_3A suspension can be significantly modified by varying the sodium salts and their dosages.

3.3 The Relation Between the Storage Modulus and Heat of Hydration

The sodium salts significantly alter the structure build-up, i.e., the increase of the storage modulus of the C_3A paste. Recently Michel et. al. proposed that the storage modulus depends on the number of contact points $f(N)$ between the particles and the stiffness of the bonds $f(\sigma)$ between the particles [59]. The stiffness of the bond between the particles depends on the stiffness and number of hydrate phases interconnecting the particles. It is reasonable to assume that the number of contacts between the large particles, i.e., quartz and C_3A, remains constant during hydration. Therefore, the structural build-up, as determined by the temporal evolution of the storage modulus G', is mainly dependent on the evolution of the bond stiffness $f(\sigma)$ between the particles. This stiffness is a function of the hydration progress, i.e., the formation of hydrate phases between the particles. Therefore, the temporal evolution of the bond stiffness is a function of the heat of hydration H, i.e., $\sigma(H)$, and an exponential relationship between the storage modulus G' and the heat of hydration H has been reported [59].

$$G' = ae^{bH} \tag{1}$$

The fitting parameter a is related to the number and geometry of particle-particle contacts in the percolated network, and b is related to the bond stiffness between the particles. Thus, equation 1 captures the different micro-structural and mechanical properties of chemically different hydrate phases. We fit the storage modulus development using equation 1 in the first 3 h of hydration (Supporting Information Figure S8). The poor fit of equation 1 to the experimental data reveals that the development of the storage modulus can not be described using a single exponential function.

Upon closer inspection, the curves appear to have up to three linear domains in the semi-logarithmic plot. This is best seen in the data for the mixture containing 1000 µmol g^{-1} of NaCl (Figure 6). The slope in the first domain (approximately between 0 – 50 J g^{-1}) is the steepest, i.e., in this hydration phase, the relative stiffness increase with progressing hydration is large in the semi-logarithmic representation. We tentatively assign this behavior to the initial formation of hydrate phases between the particles in the percolated network. While the particle network is held together by van-der-Waals forces before the

onset of hydration, the appearance of the first hydrates will bridge the particles at their contact points and, therefore, increase bond stiffness. In the second domain, the network stiffness further increases due to an increase in the number of new hydrate phases bridging the particles and the growth of the existing hydrate phases. The third domain exhibits the smallest slope. We speculate that another change in the solidification mechanism is responsible for this change in slope. Section 3.4 shows that different phases can form with progressing hydration by thermodynamically modeling the phase composition. It is beyond the scope of this study to investigate the microstructural origin of the different domains. However, we note that Michel et al. report that the hydration of C_3S in water comprises only one domain, i.e., the storage modulus can be fitted by equation 1. In contrast to the experiment of Michel, we study the hydration of C_3A with and without sodium salts. This means that we form either AFm phases or ettringite (in the case of Na_2SO_4) and AH_3 instead of C-S-H and CH. Furthermore, the chosen concentrations of the sodium salts are insufficient for the full conversion of the C_3A into the respective chloride, nitrate, or sulfate-containing AFm compounds. Consequently, depending on the sodium salt dosage, the system also forms microcrystalline $Al(OH)_3$, $C_2AH_{7.5}$ and C_4AH_{19} (see section 3.4 on thermodynamic modeling). When the chemistry of the forming hydrate phases changes, we can expect a change in the slope b. Therefore, we speculate that the difference in domains II and III might be caused by a switch to a different hydrate phase.

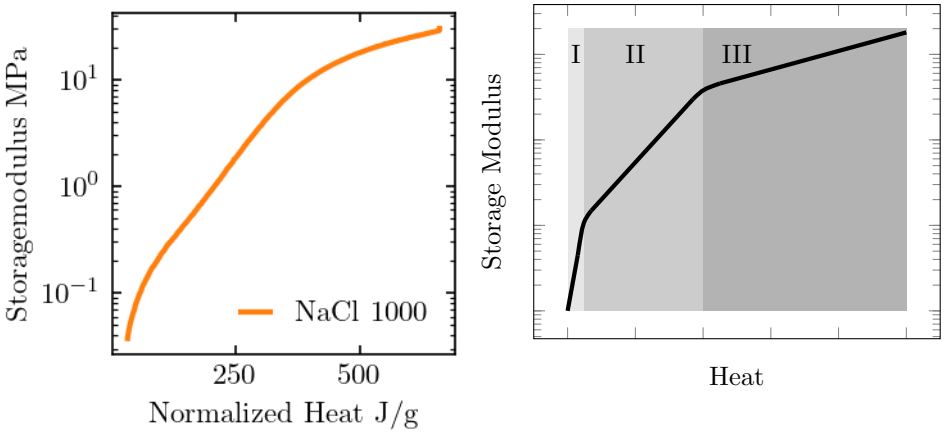

Figure 6: Storage modulus of the NaCl 1000 µmol g^{-1} sample in a semi-log diagram. Right: idealized scheme of the storage modulus development.

As we have different domains, we fit the data with a piecewise exponential function composed of two exponential functions of the type discussed above in equation 1. Although the experimental data seems composed of three domains (see above), all three are rarely distinguishable; the data often contains domains I and II or II and III (see below). Consequently, a two-domain model is reasonable for describing the data. In most experimental curves, the missing third domain, either I or III, can be explained

Table 1: Piecewise exponential fit results.

Additive	Dosage [µmol/g Binder]	a [MPa]	H_p [J/g]	Domains	b_1	b_2
Na_2SO_4	400	0.48	138.5	I/II	0.0425	0.0062
Na_2SO_4	1000	1.93	237.0	I/II	0.0384	0.0018
Na_2SO_4	2000	0.00	217.2	I	0.0375	0.0258
NaCl	400	2.33	263.4	II/III	0.0200	0.0029
NaCl	1000	2.31	371.6	II/III	0.0145	0.0039
NaCl	2000	0.00	280.4	II	0.0116	0.0079
$NaNO_3$	400	1.32	232.7	II/III	0.0136	0.0047
$NaNO_3$	1000	1.83	288.7	II/III	0.0112	0.0044
$NaNO_3$	2000	2.48	407.7	II/III	0.0122	0.0063
Reference	0	1.88	214.5	(II)/III	0.0137	0.0029

by recognizing that it is unlikely to detect phase I for the fast-reacting system. Because the rheology measurement begins after 3 min, we miss the structural development in the first three minutes. For the high concentration of Na_2SO_4, the hydration is sufficiently slowed down to reveal the large initial slope of phase I. On the other hand, our data miss the later phase III if the transition to phase III does not occur in the first three hours due to slower hydration. By fitting the piecewise function 2, we also obtain a partition point H_p, which separates the domains and use a, b_1, b_2 and H_p as fit parameters (Equation 2). The results of the fits are shown in Table 1, and the graphical representation of the fits is given in Figure 7. The fit quality is good, which underlines the usefulness of the model.

The fit values obtained by modeling are compiled in Table 1. The obtained fit values are consistent within a set of chemically similar systems, i.e., they are comparable for each added salt. For example, for $NaNO_3$, we find growing values of H_p for increasing amounts of salt added while the slopes of both fitted domains stay approximately constant. In the case of NaCl, the trend is similar; however, at the highest concentration of 2000 µmol g^{-1}, the last domain is not reached anymore within the duration of the experiment. Therefore, the value of H_p is less relevant here because the experimental data could also have been fitted with a single exponential function confirmed by the similarity of both slopes b_1 and b_2. Finally, the trend of the Na_2SO_4 containing samples is significantly different. The initial slope b_1 is much steeper with values higher than all other systems. This is most likely associated with the stronger inhibiting influence of the sulfate ion and the chemical nature of the initial hydrate phase ettringite (see next section). As the similar b_1 and b_2 values indicate, we can not clearly distinguish two separated domains at the highest sodium sulfate concentration.

$$G' = \begin{cases} ae^{b_1 H/H_p} & H \leq H_p \\ ae^{b_2 H/H_p} & H \geq H_p \end{cases} \tag{2}$$

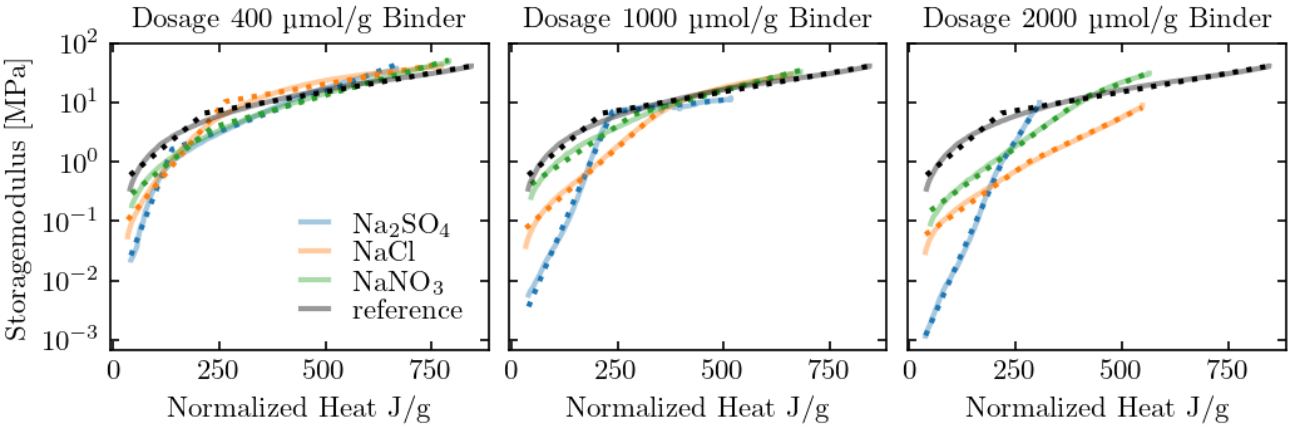

Figure 7: Storage modulus versus heat for three different concentrations of sodium salts. The fit function is shown as a dotted line; the experimental data is plotted as light, solid lines below the fit.

Table 2: Reactions of C_3A with alkali salts. Cement notation was employed where possible to keep the formulas succinct.

System	Reaction
H_2O	$2\,C_3A + 20.5\,H \longrightarrow C_4AH_{13} + C_2AH_{7.5}$
NaCl	$4\,C_3A + 36\,H + 6\,NaCl \longrightarrow 3\,C_3A \cdot CaCl_2 \cdot 10\,H + AH_3 + 6\,NaOH$
$NaNO_3$	$4\,C_3A + 36\,H + 6\,NaNO_3 \longrightarrow 3\,C_3A \cdot Ca(NO_3)_2 \cdot 10\,H + AH_3 + 6\,NaOH$
Na_2SO_4 (AFt)	$2\,C_3A + 3\,N\bar{S} + 38\,H \longrightarrow 3\,C_6A\bar{S}_3H_{32} + AH_3 + 3\,NH$
Na_2SO_4 (AFm)	$4\,C_3A + 3\,N\bar{S} + 42\,H \longrightarrow 3\,C_4A\bar{S}H_{12} + AH_3 + 3\,NH$

3.4 Thermodynamic Modeling

We model the phase evolution for the pastes comprising C_3A and sodium salt to elucidate the hydrate phases responsible for the structural build-up. We calculated the equilibrium phases for all C_3A MS mixtures with Reaktoro and the Cemdata18 database. Figure 8 depicts the equilibrium phase amounts as a function of the quantity of the dissolved C_3A, and Table 2 shows the initial reactions of the systems. The formation of the metastable AFm phases, such as C_2AH_8 ($Ca_2Al_2(OH)_{10}(H_2O)_3$), or C_4AH_{19} ($Ca_4Al_2(OH)_{14}(H_2O)_{12}$) depends on the reaction temperature. In our systems, C_4AH_{19} is predicted to form in preference to C_4AH_{13}, given the high ratio of water to C_3A ($w/C_3A = 8$) [4, 60, 61]. The thermodynamic stable product, however, is katoite (C_3AH_6, $Ca_3Al_2O_6(H_2O)_6$) [10, 62]. However, in the absence of additional ions, AFm phases are kinetically formed as the first product during the

hydration of C_3A [8, 11]. For this reason, the precipitation of katoite was not allowed to occur during the thermodynamic modeling. Furthermore, in the thermodynamic model, we did not include the quartz phase, which is present in the model system.

The introduction of sodium chloride or sodium nitrate promotes the formation of AFm-type hydrates, notably Friedel's salt ($Ca_4Al_2Cl_2(OH)_{12}(H_2O)_4$) and nitrate AFm ($Ca_4Al_2(NO_3)_2(OH)_{12}(H_2O)_4$), along with $Al(OH)_3$. After the added anion, such as nitrate, is depleted, the formation of $C_2AH_{7.5}$ is predicted, and the initially formed AH_3 dissolves again.

The addition of sodium sulfate alters the phase composition, primarily resulting in the formation of ettringite ($C_6A\bar{S}_3H_{32}$, $Ca_6Al_2(SO_4)_3(OH)_{12}(H_2O)_{26}$) and microcrystalline $Al(OH)_3$. As the sulfate ions diminish in the pore solution, ettringite consumption ensues, favoring monosulfate as the dominant hydrate phase. Given the dosages in this study, the sodium sulfate amount is insufficient for converting the entire amount of C_3A to monosulfate. Instead, at high conversions of approx. 70%, the microcrystalline AH_3 dissolves and $C_2AH_{7.5}$ formation is expected in addition to the stable monosulfate.

3.5 In-situ XRD analysis

To compare the phase assemblage obtained from the thermodynamic models with experimental findings, we conducted qualitative in-situ XRD experiments during hydration of the C_3A model suspension in the absence and presence of the sodium salts. The X-ray diffraction (XRD) patterns obtained after 3 h of hydration in the presence and absence of $NaNO_3$, NaCl, and Na_2SO_4 at a dosages of 2000 µmol g^{-1} are presented in Figure 9.

The most intense reflection of the inert quartz filler (26.4°) is similar for all samples. The main reflection of C_3A at 33.2° is reduced to varying degrees (highlighted in gray). C_3A is almost completely consumed in the reference sample after 3 h. Furthermore, the reflection of C_3A shows the highest intensity for the sample in the presence of Na_2SO_4, followed by NaCl and $NaNO_3$.

As expected, the conversion of the initially formed AFm phases to the thermodynamically stable katoite phase is not observed during the first 3 h. For the reference sample, C_2AH_8 was found to be the main hydration product (8.0°, black pentagon). The c-lattice parameter of 64.5 Å found in our sample exactly matches the value for C_2AH_8 detected by Goergens et al. in the C_2AH_x series [54]. We attempted to quantify the C_2AH_8 phase using the F-factor method described by Goergens based on the extracted scale factor. However, the resulting amount of 60 wt.% C_2AH_8 calculated based on the internal standard method (using the inert quartz filler as internal standard) [63], in combination with the F-factor method [54], is almost six times higher than the maximum amount of 11 wt.% C_2AH_8 that can precipitate if

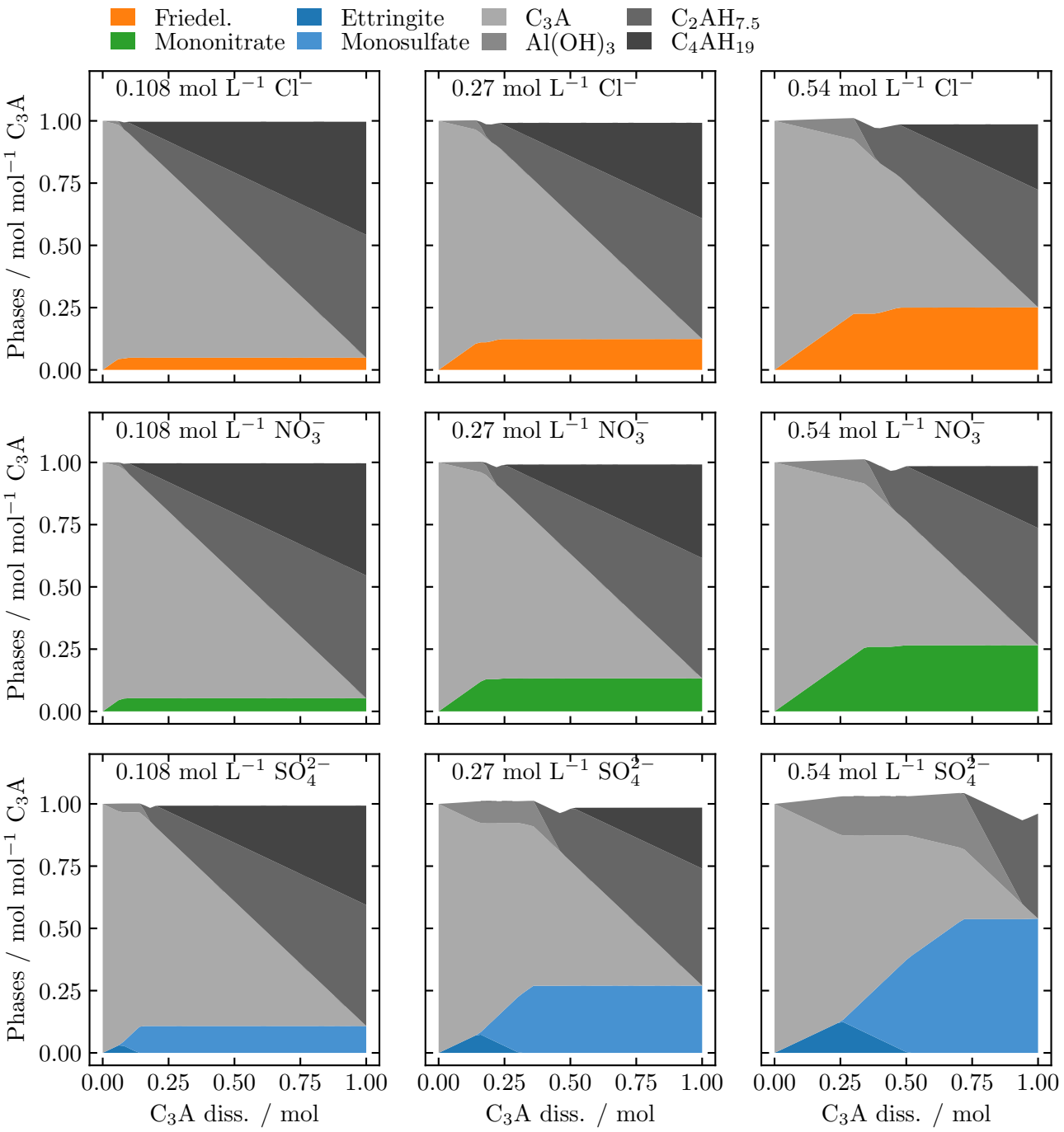

Figure 8: Phase composition dependent on dissolved C_3A for the added salts at different concentrations.

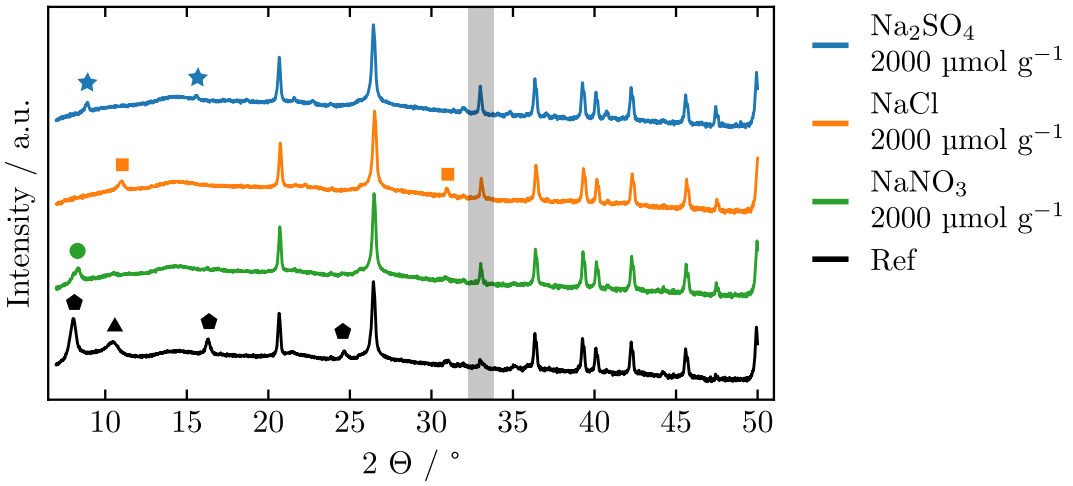

Figure 9: XRD patterns after 3 h in pure water (w/s = 0.8) and in the presence of $NaNO_3$, NaCl and Na_2SO_4 in the dosage of 2000 µmol g^{-1} C_3A. The gray area marks the main reflection of cubic C_3A at 33.2°. Marker codes to highlight the main reflections of hydrate phases: C_2AH_8 = black pentagon, monocarbonate/hemicarbonate = black triangle, nitrate AFm = green circle, Friedel's salt = orange square and ettringite = blue star.

all available C_3A (5.55 wt.%) is converted to this hydrate phase. We assume that C_2AH_8 preferentially precipitates at the interface of the polyimide film and is, therefore, over-determined compared to the other phases. Therefore, a quantification by Rietveld refinements was inaccurate for our suspension and was not further conducted for the experiments in the presence of sodium salts. Additionally, although we covered the samples with a polyimide film to prevent evaporation of the pore solution and carbonation of the sample, we also detected some hemicarbonate and monocarbonate (broad reflection between 10.0 – 11.0°) (black triangle) in the reference mixture.

In each of the three samples hydrated in the presence of sodium sulfate, chloride, or nitrate, we detect only one distinctive hydrate phase after three hours (Figure 9). Specifically, the sodium nitrate sample exhibits a reflection at 8.4° with a basal *d*-spacing of 10.5 Å (green circle). The values determined are in agreement with those described by Balonis et al. for nitrate AFm in wet conditions (≈ 100 % RH) [21]. Therefore, the formation of nitrate AFm was observed exclusively in the sodium nitrate-containing sample. The reflection at 11.0° in the sample hydrated in the sodium chloride solution can be related to the chloride containing AFm phase, Friedel's salt (orange square) [22]. Furthermore, ettringite (blue star) is the only hydrate phase precipitating after 3 h of hydration in the sodium sulfate solution, also observed, for example, by Liu et al. as hydration product of pure cubic C_3A in the presence of Na_2SO_4 (w/s = 1) [18]. Electron microscope images of the precipitated hydrate phases for all systems are provided in the Supporting Information (Figures S6 and S7). The characteristic reflection of the U-phase (at approx. 8.5°) was not observed [38, 44, 45]. Accordingly, the U-phase was excluded from the thermodynamic

modeling. Katoite was not detected during the initial 3 h hydration in any of the experiments.

In conclusion, AFm phases precipitate when C_3A hydrates in pure water or the presence of NaCl and $NaNO_3$ in the first 3 h of hydration. The main hydrates identified by XRD analysis are C_2AH_8 with pure water, Friedel's salt with NaCl, and nitrate AFm with the addition of $NaNO_3$. The presence of sodium sulfate leads to the formation of ettringite. In the presence of 2000 µmol g^{-1} of sodium salts, we could not detect the predicted AFm phases C_2AH_8 or C_4AH_{19}. Furthermore, despite being expected from the modeling, monosulfate was not detected in the first 3 h by XRD.

4 Conclusions

The control of the hydration kinetics and viscoelastic properties is critical for cementitious binders. The early properties of highly SCM-containing sustainable cements will continue to be determined by the OPC component due to its greater initial reactivity than SCM. Li et al. recently highlighted the beneficial utilization of aluminate phases in OPC systems, leading to an increased ettringite formation through a selective hydration control additive [25]. Therefore, it is essential to improve the understanding of the control over the hydration reactions of aluminate phases in OPC and their effect on kinetics and viscoelastic properties.

We used in-situ calorimetry and XRD to characterize the hydration of a C_3A model suspension containing different amounts of alkali salt. The intensity of the early C_3A hydration was attenuated in the order $Na_2SO_4 > NaCl \approx NaNO_3$. However, the initial C_3A hydration was not fully inhibited by any of the evaluated salt concentrations. The XRD analysis confirmed ettringite formation, Friedel's salt, and mononitrate in the presence of the corresponding alkali salts. However, we could not detect AH_3 or AFm phases like monosulfate and C_4AH_{19} that are predicted to form based on thermodynamic modeling.

Due to the modified hydration pathway, the sodium salts also influenced the viscoelastic properties. In contrast to the hydration of C_3S in water, the relationship between the storage modulus and the heat of hydration can not be modeled with a single exponential function. We fitted the data with a piecewise exponential function containing two exponential functions. The complex relationship between storage modulus and heat suggests that different microstructural mechanisms control the strength build-up in C_3A, alkali salt systems. The details of a multi-step stiffening reaction need to be investigated in future studies.

This study complements recent works published by other research groups (for example: [16, 27, 35, 38, 58]), as it demonstrates the ion-specific effects on C_3A hydration, accompanied by insights into phase

evolution and viscoelastic properties. It also extends the understanding of the effects of C_3A hydration and hydrate precipitation on the structural development of a cementitious model suspension. The precise control, especially of highly reactive clinker phases such as C_3A, while ensuring constant workability, can further contribute to the transition to a sustainable construction sector.

Acknowledgments

The authors would like to express their sincere gratitude to BASF Construction Additives GmbH for the generous financial support and collaboration that made this research possible.

References

[1] C. Jakob, D. Jansen, N. Ukrainczyk, E. Koenders, U. Pott, D. Stephan, J. Neubauer, "Relating Ettringite Formation and Rheological Changes during the Initial Cement Hydration: A Comparative Study Applying XRD Analysis, Rheological Measurements and Modeling", *Materials* **2019**, *12*, 2957, DOI 10.3390/ma12182957.

[2] J. Gołaszewski, "Influence of Cement Properties on Rheology of Fresh Cement Mortars without and with Superplasticizer", *Architecture Civil Engineering Environment* **2008**, 49–66.

[3] J. Beaudoin, I. Odler, "5 - Hydration, Setting and Hardening of Portland Cement" in *Lea's Chemistry of Cement and Concrete (Fifth Edition)*, (Eds.: P. C. Hewlett, M. Liska), Butterworth-Heinemann, **2019**, pp. 157–250, DOI 10.1016/B978-0-08-100773-0.00005-8.

[4] H. Taylor, *Cement Chemistry, Vol. 2nd edition*, Thomas Telford Publishing, London, **1997**, DOI 10.1680/cc.25929.

[5] S. Joseph, J. Skibsted, Ö. Cizer, "A Quantitative Study of the C3A Hydration", *Cem. Concr. Res.* **2019**, *115*, 145–159, DOI 10.1016/j.cemconres.2018.10.017.

[6] J. W. Bullard, H. M. Jennings, R. A. Livingston, A. Nonat, G. W. Scherer, J. S. Schweitzer, K. L. Scrivener, J. J. Thomas, "Mechanisms of Cement Hydration", *Cem. Concr. Res.*, Conferences Special: Cement Hydration Kinetics and Modeling (Quebec City, 2009) & CONMOD10 (Lausanne, 2010) **2011**, *41*, 1208–1223, DOI 10.1016/j.cemconres.2010.09.011.

[7] R. J. Myers, G. Geng, E. D. Rodriguez, P. da Rosa, A. P. Kirchheim, P. J. M. Monteiro, "Solution Chemistry of Cubic and Orthorhombic Tricalcium Aluminate Hydration", *Cem. Concr. Res.* **2017**, *100*, 176–185, DOI 10.1016/j.cemconres.2017.06.008.

[8] L. Black, C. Breen, J. Yarwood, C.-S. Deng, J. Phipps, G. Maitland, "Hydration of Tricalcium Aluminate (C3A) in the Presence and Absence of Gypsum—Studied by Raman Spectroscopy and X-ray Diffraction", *J. Mater. Chem.* **2006**, *16*, 1263–1272, DOI 10.1039/B509904H.

[9] A. P. Kirchheim, E. D. Rodríguez, R. J. Myers, L. A. Gobbo, P. J. M. Monteiro, D. C. C. Dal Molin, R. B. De Souza, M. A. Cincotto, "Effect of Gypsum on the Early Hydration of Cubic and Na-Doped Orthorhombic Tricalcium Aluminate", *Materials* **2018**, *11*, 568, DOI 10.3390/ma11040568.

[10] T. Hirsch, T. Matschei, D. Stephan, "The Hydration of Tricalcium Aluminate (Ca3Al2O6) in Portland Cement-Related Systems: A Review", *Cem. Concr. Res.* **2023**, *168*, 107150, DOI 10.1016/j.cemconres.2023.107150.

[11] A. C. Jupe, X. Turrillas, P. Barnes, S. L. Colston, C. Hall, D. Häusermann, M. Hanfland, "Fast in Situ X-Ray-Diffraction Studies of Chemical Reactions: A Synchrotron View of the Hydration of Tricalcium Aluminate", *Phys. Rev. B* **1996**, *53*, R14697–R14700, DOI 10.1103/PhysRevB.53.R14697.

[12] M. Collepardi, G. Baldini, M. Pauri, M. Corradi, "Tricalcium Aluminate Hydration in the Presence of Lime, Gypsum or Sodium Sulfate", *Cem. Concr. Res.* **1978**, *8*, 571–580, DOI 10.1016/0008-8846(78)90040-6.

[13] A. M. Harrisson, "4 - Constitution and Specification of Portland Cement" in *Lea's Chemistry of Cement and Concrete (Fifth Edition)*, (Eds.: P. C. Hewlett, M. Liska), Butterworth-Heinemann, Oxford, **2019**, pp. 87–155, DOI 10.1016/B978-0-08-100773-0.00004-6.

[14] J. d. S. Andrade Neto, A. G. De la Torre, A. P. Kirchheim, "Effects of Sulfates on the Hydration of Portland Cement – A Review", *Constr. Build. Mater.* **2021**, *279*, 122428, DOI 10.1016/j.conbuildmat.2021.122428.

[15] G. Geng, R. J. Myers, Y.-S. Yu, D. A. Shapiro, R. Winarski, P. E. Levitz, D. A. L. Kilcoyne, P. J. M. Monteiro, "Synchrotron X-ray Nanotomographic and Spectromicroscopic Study of the Tricalcium Aluminate Hydration in the Presence of Gypsum", *Cem. Concr. Res.* **2018**, *111*, 130–137, DOI 10.1016/j.cemconres.2018.06.002.

[16] A. S. Brand, S. B. Feldman, P. E. Stutzman, A. V. Ievlev, M. Lorenz, D. C. Pagan, S. Nair, J. M. Gorham, J. W. Bullard, "Dissolution and Initial Hydration Behavior of Tricalcium Aluminate in Low Activity Sulfate Solutions", *Cem. Concr. Res.* **2020**, *130*, 105989, DOI 10.1016/j.cemconres.2020.105989.

[17] H. Minard, S. Garrault, L. Regnaud, A. Nonat, "Mechanisms and Parameters Controlling the Tricalcium Aluminate Reactivity in the Presence of Gypsum", *Cem. Concr. Res.* **2007**, *37*, 1418–1426, DOI 10.1016/j.cemconres.2007.06.001.

[18] X. Liu, P. Feng, C. Lyu, S. Ye, "The Role of Sulfate Ions in Tricalcium Aluminate Hydration: New Insights", *Cem. Concr. Res.* **2020**, *130*, 105973, DOI 10.1016/j.cemconres.2020.105973.

[19] R. J. Myers, G. Geng, J. Li, E. D. Rodríguez, J. Ha, P. Kidkhunthod, G. Sposito, L. N. Lammers, A. P. Kirchheim, P. J. M. Monteiro, "Role of Adsorption Phenomena in Cubic Tricalcium Aluminate Dissolution", *Langmuir* **2017**, *33*, 45–55, DOI 10.1021/acs.langmuir.6b03474.

[20] D. Axthammer, M. Ordynska, T. Gädt, "C3A Variation in Synthetic Model Cements - Influence on Rheology and Reactivity", *ce/papers* **2023**, *6*, 670–676, DOI 10.1002/cepa.2806.

[21] M. Balonis, M. Mędala, F. P. Glasser, "Influence of Calcium Nitrate and Nitrite on the Constitution of AFm and AFt Cement Hydrates", *Adv. Cem. Res.* **2011**, *23*, 129–143, DOI 10.1680/adcr.10.00002.

[22] G. Renaudin, F. Kubel, J. .-. Rivera, M. Francois, "Structural Phase Transition and High Temperature Phase Structure of Friedels Salt, 3CaO · Al2O3 · CaCl2 · 10H2O", *Cem. Concr. Res.* **1999**, *29*, 1937–1942, DOI 10.1016/S0008-8846(99)00199-4.

[23] J. Plank, D. Zhimin, H. Keller, F. v. Hössle, W. Seidl, "Fundamental Mechanisms for Polycarboxylate Intercalation into C3A Hydrate Phases and the Role of Sulfate Present in Cement", *Cem. Concr. Res.* **2010**, *40*, 45–57, DOI 10.1016/j.cemconres.2009.08.013.

[24] L. G. Baquerizo, T. Matschei, K. L. Scrivener, M. Saeidpour, L. Wadsö, "Hydration States of AFm Cement Phases", *Cem. Concr. Res.* **2015**, *73*, 143–157, DOI 10.1016/j.cemconres.2015.02.011.

[25] X. Li, H. Grassl, C. Hesse, J. Dengler, "Unlocking the Potential of Ordinary Portland Cement with Hydration Control Additive Enabling Low-Carbon Building Materials", *Commun. Mater.* **2024**, *5*, 1–9, DOI 10.1038/s43246-023-00441-9.

[26] T. Liberto, A. Nenning, M. Bellotto, M. C. Dalconi, D. Dworschak, L. Kalchgruber, A. Robisson, M. Valtiner, J. Dziadkowiec, "Detecting Early-Stage Cohesion Due to Calcium Silicate Hydration with Rheology and Surface Force Apparatus", *Langmuir* **2022**, *38*, 14988–15000, DOI 10.1021/acs.langmuir.2c02783.

[27] T. Huang, Q. Yuan, F. He, Y. Xie, "Understanding the Mechanisms behind the Time-Dependent Viscoelasticity of Fresh C3A–Gypsum Paste", *Cem. Concr. Res.* **2020**, *133*, 106084, DOI 10.1016/j.cemconres.2020.106084.

[28] N. Roussel, G. Ovarlez, S. Garrault, C. Brumaud, "The Origins of Thixotropy of Fresh Cement Pastes", *Cement and Concrete Research* **2012**, *42*, 148–157, DOI 10.1016/j.cemconres.2011.09.004.

[29] N. Roussel, H. Bessaies-Bey, S. Kawashima, D. Marchon, K. Vasilic, R. Wolfs, "Recent Advances on Yield Stress and Elasticity of Fresh Cement-Based Materials", *Cem. Concr. Res.* **2019**, *124*, 105798, DOI 10.1016/j.cemconres.2019.105798.

[30] T. Mezger, *Angewandte Rheologie*, 5. Aufl., Anton Paar, Graz, **2020**.

[31] A. M. Mostafa, A. Yahia, "Physico-Chemical Kinetics of Structural Build-up of Neat Cement-Based Suspensions", *Cem. Concr. Res.* **2017**, *97*, 11–27, DOI 10.1016/j.cemconres.2017.03.003.

[32] Q. Yuan, D. Zhou, K. H. Khayat, D. Feys, C. Shi, "On the Measurement of Evolution of Structural Build-up of Cement Paste with Time by Static Yield Stress Test vs. Small Amplitude Oscillatory Shear Test", *Cem. Concr. Res.* **2017**, *99*, 183–189, DOI 10.1016/j.cemconres.2017.05.014.

[33] Q. Yuan, X. Lu, K. H. Khayat, D. Feys, C. Shi, "Small Amplitude Oscillatory Shear Technique to Evaluate Structural Build-up of Cement Paste", *Mater. Struct.* **2016**, *50*, 112, DOI 10.1617/s11527-016-0978-2.

[34] P. Bénard, S. Garrault, A. Nonat, C. Cau-Dit-Coumes, "Hydration Process and Rheological Properties of Cement Pastes Modified by Orthophosphate Addition", *J. Am. Ceram. Soc.* **2005**, *25*, 1877–1883, DOI 10.1016/j.jeurceramsoc.2004.06.017.

[35] K. Han, T. Guo, X. Shu, Q. Ran, Y. Guo, J. Shi, "Insight into the Role of Early C3A Hydration in Structural Build-up of Cement Paste", *Cem. Concr. Res.* **2024**, *175*, 107354, DOI 10.1016/j.cemconres.2023.107354.

[36] D. Axthammer, T. Lange, J. Dengler, T. Gädt, "Kilogram Scale Synthesis of C3A Polymorphs and Their Hydration Reactions", *Cement* **2023**, *12*, DOI 10.1016/j.cement.2023.100064.

[37] S. Pourchet, L. Regnaud, J. P. Perez, A. Nonat, "Early C3A Hydration in the Presence of Different Kinds of Calcium Sulfate", *Cem. Concr. Res.* **2009**, *39*, 989–996, DOI 10.1016/j.cemconres.2009.07.019.

[38] J. S. Andrade Neto, P. R. de Matos, A. G. De la Torre, C. E. M. Campos, P. J. P. Gleize, P. J. M. Monteiro, A. P. Kirchheim, "The Role of Sodium and Sulfate Sources on the Rheology and Hydration of C3A Polymorphs", *Cem. Concr. Res.* **2022**, *151*, 106639, DOI 10.1016/j.cemconres.2021.106639.

[39] T. Liberto, M. L. Merrer, C. Barentin, M. Bellotto, J. Colombani, "Elasticity and Yielding of a Calcite Paste: Scaling Laws in a Dense Colloidal Suspension", *Soft Matter* **2017**, *13*, 2014–2023, DOI 10.1039/C6SM02607A.

[40] T. Lange, D. Axthammer, D. Jansen, T. Gädt, "The First 15 Minutes of Portland Cement Hydration - A Benchmarking Study of In-situ Mixers for Isothermal Heat Flow Calorimetry", **submitted**.

[41] A.M.M. Leal, *Reaktoro: An open-source unified framework for modeling chemically reactive systems.* Version 2.11.

[42] B. Lothenbach, D. A. Kulik, T. Matschei, M. Balonis, L. Baquerizo, B. Dilnesa, G. D. Miron, R. J. Myers, "Cemdata18: A Chemical Thermodynamic Database for Hydrated Portland Cements and Alkali-Activated Materials", *Cem. Concr. Res.* **2019**, *115*, 472–506, DOI 10.1016/j.cemconres.2018.04.018.

[43] B. Lothenbach, L. Pelletier-Chaignat, F. Winnefeld, "Stability in the System CaO–Al2O3–H2O", *Cem. Concr. Res.* **2012**, *42*, 1621–1634, DOI 10.1016/j.cemconres.2012.09.002.

[44] G. Li, P. Le Bescop, M. Moranville-Regourd, "Synthesis of the U Phase (4CaO . 0.9Al2O3 . 1.1SO3 . 0.5Na2O . 16H2O)", *Cem. Concr. Res.* **1997**, *27*, 7–13, DOI 10.1016/S0008-8846(96)00194-9.

[45] G. Li, P. Le Bescop, M. Moranville, "The U Phase Formation in Cement-Based Systems Containing High Amounts of Na2SO4", *Cem. Concr. Res.* **1996**, *26*, 27–33, DOI 10.1016/0008-8846(95)00189-1.

[46] A. A. Coelho, "TOPAS and TOPAS-Academic: An Optimization Program Integrating Computer Algebra and Crystallographic Objects Written in C++", *J. Appl. Cryst.* **2018**, *51*, 210–218, DOI 10.1107/S1600576718000183.

[47] P. Mondal, J. W. Jeffery, "The Crystal Structure of Tricalcium Aluminate, Ca3Al2O6", *Acta Crystallogr. Sect. B* **1975**, *31*, 689–697, DOI 10.1107/S0567740875003639.

[48] Y. Le Page, G. Donnay, "Refinement of the Crystal Structure of Low-Quartz", *Acta Crystallogr. Sect. B* **1976**, *32*, 2456–2459, DOI 10.1107/S0567740876007966.

[49] F. Goetz-Neunhoeffer, J. Neubauer, "Refined Ettringite (Ca6Al2(SO4)3(OH)12•26H2O) Structure for Quantitative X-ray Diffraction Analysis", *Powder Diffr.* **2006**, *21*, 4–11, DOI 10.1154/1.2146207.

[50] A. Terzis, S. Filippakis, H.-J. Kuzel, H. Burzlaff, "The crystal structure of Ca2Al(OH)6Cl · 2H2O", *Z. Kristallogr. Cryst. Mater* **1987**, *181*, 29–34, DOI 10.1524/zkri.1987.181.14.29.

[51] G. Renaudin, M. François, "The Lamellar Double-Hydroxide (LDH) Compound with Composition 3CaO.Al2O3.Ca(NO3)2. *Acta Crystallogr. Sect. C* **1999**, *55*, 835–838, DOI 10.1107/S0108270199003066.

[52] M. François, G. Renaudin, O. Evrard, "A Cementitious Compound with Composition 3CaO.Al2O3.CaCO3.11H2O", *Acta Crystallogr. Sect. C* **1998**, *54*, 1214–1217, DOI 10.1107/S0108270198004223.

[53] T. Runčevski, R. E. Dinnebier, O. V. Magdysyuk, H. Pöllmann, "Crystal Structures of Calcium Hemicarboaluminate and Carbonated Calcium Hemicarboaluminate from Synchrotron Powder Diffraction Data", *Acta Crystallogr. Sect. B* **2012**, *68*, 493–500, DOI 10.1107/S010876811203042X.

[54] J. Goergens, A. Koehler, F. Goetz-Neunhoeffer, "Calibration and Quantitative Analysis of C2AHx (2CaO·Al2O3·xH2O) by Rietveld Refinement Combined G-factor Method", *Cem. Concr. Res.* **2022**, *158*, 106854, DOI 10.1016/j.cemconres.2022.106854.

[55] S. T. Bergold, F. Goetz-Neunhoeffer, J. Neubauer, "Quantitative Analysis of C–S–H in Hydrating Alite Pastes by in-Situ XRD", *Cem. Concr. Res.* **2013**, *53*, 119–126, DOI 10.1016/j.cemconres.2013.06.001.

[56] S. Mantellato, M. Palacios, R. J. Flatt, "Impact of Sample Preparation on the Specific Surface Area of Synthetic Ettringite", *Cem. Concr. Res.* **2016**, *86*, 20–28, DOI 10.1016/j.cemconres.2016.04.005.

[57] R. Snellings, J. Chwast, Ö. Cizer, N. De Belie, Y. Dhandapani, P. Durdzinski, J. Elsen, J. Haufe, D. Hooton, C. Patapy, M. Santhanam, K. Scrivener, D. Snoeck, L. Steger, S. Tongbo, A. Vollpracht, F. Winnefeld, B. Lothenbach, "RILEM TC-238 SCM Recommendation on Hydration Stoppage by Solvent Exchange for the Study of Hydrate Assemblages", *Mater. Struct.* **2018**, *51*, 172, DOI 10.1617/s11527-018-1298-5.

[58] S. Ye, P. Feng, Y. Liu, J. Liu, J. W. Bullard, "Dissolution and Early Hydration of Tricalcium Aluminate in Aqueous Sulfate Solutions", *Cem. Concr. Res.* **2020**, *137*, 106191, DOI 10.1016/j.cemconres.2020.106191.

[59] L. Michel, L. Reiter, A. Sanner, R. J. Flatt, D. S. Kammer, Structural Build-up at Rest in the Induction and Acceleration Periods of OPC, **2024**, DOI 10.48550/arXiv.2404.02850.

[60] P. Meredith, A. M. Donald, N. Meller, C. Hall, "Tricalcium Aluminate Hydration: Microstructural Observations by in-Situ Electron Microscopy", *J. Mater. Sci.* **2004**, *39*, 997–1005, DOI 10.1023/B:JMSC.0000012933.74548.36.

[61] A. N. Christensen, T. R. Jensen, N. V. Y. Scarlett, I. C. Madsen, J. C. Hanson, "Hydrolysis of Pure and Sodium Substituted Calcium Aluminates and Cement Clinker Components Investigated by in Situ Synchrotron X-ray Powder Diffraction", *J. Am. Ceram. Soc.* **2004**, *87*, 1488–1493, DOI 10.1111/j.1551-2916.2004.01488.x.

[62] E. Breval, "C3A Hydration", *Cem. Concr. Res.* **1976**, *6*, 129–137, DOI 10.1016/0008-8846(76)90057-0.

[63] R. Snellings, "X-Ray Powder Diffraction Applied to Cement" in *A Practical Guide to Microstructural Analysis of Cementitious Materials*, CRC Press, Boca Raton, **2016**, pp. 108–176, DOI 10.1201/b19074.